Smoothness-constrained Dynamic Parameter Estimation for InSAR Time Series

Yuqing Wang, Wietske S. Brouwer, Freek J. van Leijen, and Ramon F. Hanssen

***Abstract*—Urban resilience and decision-making rely on continuous monitoring of key safety indicators. The increasing availability of interferometric SAR (InSAR) observations offers a valuable opportunity for near real-time stability monitoring, particularly in the built environment. However, traditional InSAR time series methods use batch processing to estimate static displacement parameters, limiting early anomaly detection, computational efficiency, and use of ongoing SAR data. These methods also assume motion behavior remains constant over time. Here we introduce a new method—DYNamic parAMeter estimation of InSAR scaTterer motion in near-real timE (DYNAMITE)—that enables instantaneous parameter estimation by capturing dynamic behavior in InSAR time series. The method uses a state-vector prediction model updated with new observations via recursive least squares, eliminating the need to store past data. It imposes a smoothness constraint on displacement based on an exponentially correlated velocity model assuming an Ornstein-Uhlenbeck process and uses normalized median amplitude dispersion as a quality metric. Smoothness is controlled by specifying the instantaneous velocity's standard deviation and decorrelation time. Results show the recursive approach matches batch methods in quality while better capturing dynamic behavior, supporting near real-time monitoring.**

***Index Terms*—InSAR point scatterers, dynamic parameter estimation, recursive least squares, smoothness constraints, near real-time monitoring**

I. Introduction

Synthetic aperture radar interferometry (InSAR) enables precise monitoring of surface and infrastructure stability. However, conventional InSAR methods are built for *batch* processing, using static SAR datasets to estimate a predefined static set of parameters [1], [2], [3], [4]—unsuited for dynamic, real-time monitoring with continuous measurement updates. These methods assume all scatterers follow the same limited, time-invariant models, which is unrealistic in complex urban areas where conditions frequently change. This static approach lacks discriminatory power to detect changes in kinematic behavior and is computationally inefficient as new data arrives. Starting from the parameter estimation between *arcs* connecting two points, conventional batch processing uses a spatial network integration in order to connect all arcs to a reference point, to produce a geospatial (map) visualization of the estimated parameters. Yet, for detecting changes in dynamic behavior, there is no pressing need to produce map visualizations, as the detection may as well be performed on single arcs. Moreover, subsequent batch processing of an expanding time series, here referred to as the *incremental batch* approach, fails to provide a 'memory' of earlier results, causing problems in the interpretation, and a polynomial increase in computation time and disk storage. Finally, conventional batch processing methodologies fail to account for quality differences between scatterers. Typically, the degree of fit between the model, defined by fixed parameters, and the observations—often somewhat unfavorably termed temporal coherence—is used as a post hoc quality metric. However, this approach conflates model imperfections with observational noise, making unambiguous interpretation difficult.

These sub-optimal characteristics of batch InSAR processing call for the development of an alternative approach that optimally adapts to temporal variability. This approach should determine a time-varying parameterization based on individual arcs, operate recursively while efficiently storing previous evaluations, and incorporate quality control.

From a parameter estimation perspective, all time-series InSAR methods are inherently ill-posed, yielding an infinite number of potential solutions [5]. This arises from the unknown integer ambiguities associated with each observation, compounded by the need to estimate certain physical or geometrical parameters of the signal. The conventional approach assumes that parameterization remains constant over time, which limits flexibility. Therefore, imposing smoothness conditions on the dynamic behavior is essential to constrain the solution space [6], [7]. This can be done implicitly or explicitly. Conventionally, temporal smoothness is enforced implicitly, by choosing a functional model with a limited set of parameters, e.g. linear, low-order polynomials, periodic, and temperature-based models. In fact, the default 'constant velocity model' should be regarded as equivalent to 'assuming infinite smoothness'. Approaches to adaptively select and test more complex displacement models have been proposed [3], [4], while multiple hypothesis tests have been suggested to find an optimal kinematic model from a library of canonical functions in an a posterior step [8]. The choice for the models forces solutions to obey the pre-imposed implicit smoothness criteria. Thus, only results sufficiently satisfying those models will be accepted and visualized, while deviating dynamic behavior will be erroneously discarded as 'noise'. Yet, from a practical point of view, these points may indeed be the ones most interesting and relevant. Here we propose to work with explicit smoothness criteria. By communicating smoothness criteria explicitly, specific for particular use cases, we make them subject to scrutiny and debate, and we can investigate the impact of either more progressive or conservative smoothness

The authors are with the Department of Geoscience and Remote Sensing, Delft University of Technology, Delft, 2628 CN, The Netherlands (email: y.wang-29@tudelft.nl, w.s.brouwer@tudelft.nl, f.j.vanleijen@tudelft.nl, r.f.hanssen@tudelft.nl).

criteria.

Recursive processing has been proposed in InSAR time series analysis towards near real-time monitoring [9], [10], [11], [12], [13]. Verburg [14] introduced a recursive estimator based on the Kalman filter for both parameter and ambiguity estimation, incorporating a temporal smoothness constraint. Ansari et al. [15] developed a sequential estimator to efficiently achieve phase-linking, optimizing the phase time series of distributed scatterers sequentially. Dalaison and Jolivet [16] proposed a Kalman filter approach for InSAR time series analysis, utilizing a parameterized model defined as a linear combination of user-defined functions to solve for the temporal evolution of phase changes. Hu et al. [17] presented a method for estimating (static) parameters, such as constant velocity in the displacement model, by updating them with new phase observations through a static Kalman filter.

In this study, we present a novel framework for the recursive estimation of motion-related parameters in InSAR time series, incorporating explicit constraints on signal smoothness to enhance robustness and interpretability: DYNamic parAMeter estimation of InSAR scaTterer motion in near-real timE (DYNAMITE). In Section II, we introduce the method for the initialization step of the procedure, followed by the recursive least-squares method for the parameter update in Section III. Results for the batch and recursive solutions are presented in Sections IV, followed by the conclusion in Section V.

II. Initialization for parameter estimation

Prior to initiating the recursive update procedure, an initialization is performed using an initial set of SAR acquisitions. This initialization is based on individual arcs, which are defined as quasi-vectors connecting a base point (i) to a companion point (j). Below, we present a generic model for initial parameterization and ambiguity resolution using integer least squares (ILS), followed by a specific model formulation that explicitly defines the unknown parameters to be estimated, using amplitude data as a proxy quality metric for phase estimation.

A. Generic model formulation

For a specific PS[1] j, we denote the single look complex (SLC) phase of the daughter[2] image at epoch t relative to the phase of the mother image (at a reference epoch t_0) as the temporal single-difference observation $\psi_j^{t_0 t}$. Here, $t = 1, ..., m_1, m_1+1, ..., m_1+m_2$, where m_1 and m_2 denote the number of observations used in the initialization and update process, respectively, as elaborated further in Section III-A. The modulo-2π ('wrapped') phase for PS j relative to a base point i is referred to as the spatio-temporal double-difference (DD) observation, $\underline{\varphi}_{ij}^{t_0 t} \in [-\pi, +\pi)$, obtained by complex multiplication. As the absolute (non-modulo-2π) DD phase observation $\underline{\phi} \in \mathbb{R}$ is not available, we apply ILS [21] to estimate the integer ambiguities. The functional and stochastic model for an arc can be written as [22]

$$\begin{aligned} E\{\begin{bmatrix} \underline{\varphi} \\ \underline{b}_0 \end{bmatrix}\} &= \begin{bmatrix} \mathbf{F_1} & \mathbf{B}_1 \\ \mathbf{F_2} & \mathbf{B}_2 \end{bmatrix} \begin{bmatrix} f \\ b \end{bmatrix}; \text{ and} \\ D\{\begin{bmatrix} \underline{\varphi} \\ \underline{b}_0 \end{bmatrix}\} &= \begin{bmatrix} Q_\varphi & 0 \\ 0 & Q_{b_0} \end{bmatrix}, \end{aligned} \tag{1}$$

where $E\{.\}$ is the expectation operator, $\underline{\varphi} \in [-\pi, +\pi)$ is the vector of m_1 DD phase observations, and $\underline{b}_0$ are pseudo-observations. $D\{.\}$ is the dispersion of the observables described by the corresponding variance-covariance matrices (VCM) Q_φ and Q_{b_0}. f is the vector of the m_1 unknown integer ambiguities ($f \in \mathbb{Z}$), and b is the vector of n unknown parameters of interest, discussed in detail in Sec. II-B. For each parameter of interest in b, a pseudo-observation is added in $\underline{b}_0$. The pseudo observations $\underline{b}_0$ are required to solve the model rank-deficiency. $\mathbf{F_1}$ is an $m_1 \times m_1$ diagonal matrix with -2π on the diagonal, $\mathbf{B}_1$ is an $m_1 \times n$ matrix that transforms the parameters b into the expectation of the absolute DD phase observations $\underline{\phi}$, $\mathbf{F_2}$ is an $n \times m_1$ zero matrix, and $\mathbf{B}_2$ is an $n \times n$ identity matrix. The float solution $\underline{\hat{c}}$ (i.e., disregarding the integerness of f) and the accompanying VCM $Q_{\hat{c}}$ are obtained using least-squares and denoted as

$$\underline{\hat{c}} = \begin{bmatrix} \underline{\hat{f}} \\ \underline{\hat{b}} \end{bmatrix}; \quad Q_{\hat{c}} = \begin{bmatrix} Q_{\hat{f}} & Q_{\hat{f}\hat{b}} \\ Q_{\hat{b}\hat{f}} & Q_{\hat{b}} \end{bmatrix}. \tag{2}$$

Subsequently, the integer ambiguities $\check{f}$ are estimated after optimizing the ambiguity search spaces with the Least-squares AMBiguity Decorrelation Adjustment (LAMBDA) algorithm [21]. The fixed ambiguities are subsequently used to obtain the solution of the unknowns $\underline{\check{b}}$ and the corresponding VCM $Q_{\check{b}}$ by [23]

$$\begin{aligned} \underline{\check{b}} &= \underline{\hat{b}} - Q_{\hat{b}\hat{f}} Q_{\hat{f}}^{-1} (\hat{f} - \check{f}); \\ Q_{\check{b}} &= Q_{\hat{b}} - Q_{\hat{b}\hat{f}} Q_{\hat{f}}^{-1} Q_{\hat{f}\hat{b}}. \end{aligned} \tag{3}$$

Thus, $\underline{\check{b}}$ and $Q_{\check{b}}$ are the required initial values for starting the recursive update, elaborated below.

B. Specific model formulation

We consider the modulo-2π DD phase $\underline{\varphi}_{ij}^{t_0 t}$ between PS j and base point i, over the time interval from epoch t_0 to t as

$$\underline{\varphi}_{ij}^{t_0 t} = \underline{\phi}_D + \underline{\phi}_{\Delta H} + \underline{\phi}_\mu + \underline{\phi}_{\text{n}} + 2\pi\, f, \text{ with } f \in \mathbb{Z}, \tag{4}$$

where $\underline{\phi}_D$, $\underline{\phi}_{\Delta H}$, $\underline{\phi}_\mu$, and $\underline{\phi}_{\text{n}}$ represent the phase components between points i and j over the time interval t_0 to t, attributed to displacement, cross-range distance, thermal expansion, and noise, respectively, and the last term shows the ambiguity. The vector of unknown parameters b is

$$b = \begin{bmatrix} v & \Delta H & \eta & S \end{bmatrix}^\intercal, \tag{5}$$

[1]While the method is discussed for point scatterers (PS), it can be easily extended to distributed scatterers (DS) [18], [19], [20].

[2]We refer to 'mother and daughters,' where the mother image is defined as the reference image.

where v is a constant linear displacement rate[3], ΔH is the cross-range distance[4], and η is the arc's thermal expansion factor reacting proportionally to temperature change, following from [25]

$$\eta = \mu_{\Delta K_t} \cdot L_{\text{LOS}}, \tag{6}$$

where $\mu_{\Delta K_t}$ is the linear expansion coefficient, i.e., a material property, and L_{LOS} is the dimension of the object in the LOS direction. The last parameter S denotes the phase constant that corresponds to the atmospheric delay and scattering noise difference in the mother image. In the absence of prior knowledge, the pseudo observations $\underline{b}_0$ are set to zero and the VCM Q_{b_0} contains a-priori chosen variances which provide soft bounds to the range of possible values for the parameters of interest b.

In Eq. (1), $\mathbf{B}_1$ transforms the parameters b into the expectation of the absolute DD phase observations $\underline{\phi}$, with

$$\mathbf{B}_1 = \begin{bmatrix} -\frac{4\pi}{\lambda}t & -\frac{4\pi}{\lambda}\frac{B_t^{\perp}}{R} & -\frac{4\pi}{\lambda}\Delta K_t & -\frac{4\pi}{\lambda} \end{bmatrix}, \tag{7}$$

where $4\pi/\lambda$ converts distance to phase, using the wavelength λ of the radar. The perpendicular baseline $B_t^{\perp}$ is evaluated between the mother and daughter image at epoch t, and the range R is defined from the mother orbit. The ratio $B_t^{\perp}/R$ of the perpendicular baseline and the range is computed for the companion point. The first entry reflects a constant velocity model, used in this initialization stage only. The second entry relates the cross-range distance to the phase observable, while the third entry refers to the relative temperature change $\Delta K_t \equiv \Delta K_{t_0 t}$ between epoch t and the reference epoch t_0. The last entry relates the atmospheric delay and the scattering noise to the phase observable.

We assume no correlation between DD phase observations since (i) every resolution cell is unique, with its own scattering mechanisms, and the time-variant clutter is uncorrelated between different resolution cells and epochs [26]; (ii) the effect of the mother image is accounted for in the functional model and is characterized by the offset S; (iii) the displacement is well covered in the functional model, this is the part of the signal of interest and should therefore not be captured in the stochastic model; and (iv) atmospheric signal delays are uncorrelated across different epochs. Thus, the VCM of the DD phase observations Q_φ can be represented as a diagonal matrix and simplified to

$$\begin{aligned} Q_\varphi &= (\sigma_{\varphi_i}^2 + \sigma_{\varphi_j}^2)\mathbf{I}_{m_1} \\ &= \sigma_{\varphi_{ij}}^2 \mathbf{I}_{m_1}, \end{aligned} \tag{8}$$

where $\mathbf{I}_{m_1}$ is an identity matrix of size equal to the number of observations, σ_{φ_i}, σ_{φ_j} and $\sigma_{\varphi_{ij}}$ are the a-priori standard deviations of the phase of point i, point j and arc ij, respectively. These values can be approximated by the normalized amplitude dispersion (NAD) [2], [27]

$$\sigma_\varphi \approx \frac{\sigma_a}{\mu_a} = \text{NAD}, \tag{9}$$

where a is the vector of the amplitude time series, μ_a is its mean, and σ_a its standard deviation. Potentially, a distance-dependent term can be included as well, see [27]. Since the NAD is sensitive to outliers, especially in the built environment, leading to an overly pessimistic estimate of the phase quality, we use instead the normalized median absolute deviation (NMAD) of the amplitude vector a, defined by M_a [27]

$$\text{M}_a = \frac{\text{med}(|a - \text{med}(a)|)}{\text{med}(a)}, \tag{10}$$

where $\text{med}(a)$ is the median of the amplitude time series vector a. The derived empirical relation between the NMAD and σ_φ is defined conservatively as [27]

$$\sigma_\varphi = 1.3\,\text{M}_a + 1.9\,\text{M}_a^2 + 11.6\,\text{M}_a^3. \tag{11}$$

Herewith, σ_{φ_i} and σ_{φ_j} can be computed respectively to estimate $\sigma_{\varphi_{ij}}$, see Eq. (8).

III. Recursive update

Here we present the mathematical model for parameter updating using recursive least-squares, introducing a new dynamic parameterization and a smoothness constraint based on correlated velocity, consequently, correlated displacement. We outline how to incorporate new ('incoming') observations (wrapped phases) to the existing time series. Subsequently, we demonstrate the processing scheme tailored for InSAR point scatterers, including incremental batch processing, full batch processing, and recursive processing.

A. Dynamic processing

In the initialization stage, see Section II, we applied the conventional assumption that the parameters are static, which is not realistic for most cases. Especially when time series are longer, and/or when the object of study can be considered less rigid, we prefer time-varying parameters, to be estimated in recursive form. To allow for changes in the dynamic behavior of a point, we need to introduce velocity as a new parameter. Thus, to model this dynamic behavior, we consider the *instantaneous* state vector of the unknowns, i.e., instantaneous position, and instantaneous velocity, reformulating the first elements in the vector of unknown parameters, cf. Eq. (5), to

$$x_t = \begin{bmatrix} P_t & v_t & \Delta H_t & \eta_t \end{bmatrix}^\top, \tag{12}$$

where $P_t \equiv P_{t_0 t}$ is the instantaneous LoS position at epoch t, relative to its position at the reference epoch t_0, (hence, it represents a change in position, i.e., a displacement), while v_t is the instantaneous LoS velocity at epoch t, respectively.[5]

[3]The assumption of a constant average velocity is used only in first approximation for the initialization phase. Its applicability needs to be evaluated per case.

[4]Note that this is different from the conventional 'DEM-error' [24], as it is not an elevation in vertical direction.

[5]Since our approach is tailored towards the monitoring of short arcs we currently disregard the atmospheric noise.

While including v_t in this vector may seem superfluous at first glance—since P_t already describes the relative position signal and velocity can be considered the derivative of the position—both parameters should be regarded as non-related parameters that are estimated independently, and *not* as merely derivatives of the position. Thus the design matrix will become

$$\mathbf{A_t} = \left[\; -\tfrac{4\pi}{\lambda} \quad 0 \quad -\tfrac{4\pi}{\lambda}\tfrac{B_t^{\perp}}{R} \quad -\tfrac{4\pi}{\lambda}\Delta K_t \; \right]. \tag{13}$$

The first entry transforms the position P_t into radians. The second entry is null since the position is captured in P_t, while v_t is not yet relevant in the expectation of $\underline{\phi}_t$. The initial values for state vector $\underline{\hat{x}}_0$ and the corresponding VCM $Q_{\hat{x}_0}$—equal to $\underline{\check{b}}$ and $Q_{\check{b}}$, respectively— can be computed with Eq. (3). We now rename the estimator $\underline{\hat{x}}_t$ to $\underline{\hat{x}}_{t|t}$, i.e.,

the estimator at epoch t, given the time series data until and including epoch t. The important computational consequence for computing the latest least-squares estimator $\underline{\hat{x}}_{t|t}$ is that there is no need to store the previous observables $[\underline{\phi}_1, \ldots, \underline{\phi}_{t-1}]$. That is, once the initial $\underline{\hat{x}}_t$ is known, the updated estimator $\underline{\hat{x}}_{t|t}$ can be recursively computed from (i) the previous estimator, $\underline{\hat{x}}_{t-1|t-1}$, (ii) its corresponding VCM $Q_{\hat{x}_{t-1|t-1}}$, and (iii) the new observation $\underline{\phi}_t$.

The prediction of the state vector from the previous epoch $t-1$ to the current epoch t, here referred to as the *state transition*,

$$\underline{\hat{x}}_{t|t-1} = \Phi_{t,t-1}\, \underline{\hat{x}}_{t-1|t-1}, \tag{14}$$

where $\Phi_{t,t-1}$ is an $n \times n$ transition matrix that relates the estimated parameters $\underline{\hat{x}}_{t-1}$ for epoch $t-1$, to the predicted values of these parameters $\underline{\hat{x}}_t$ at epoch t in the future. The exact formulation of the transition matrix will be elaborated below; for now we consider it as given.

Eq. (14) requires the assumption that the state transition can be adequately described with a single matrix, $\Phi_{t,t-1}$. Obviously, this will not be realistic for most practical applications. To relax this assumption and 'close' the equation, we add a *dynamics vector*, $d_{t,t-1}$, denoted $\underline{d}_t \equiv \underline{d}_{t,t-1}$ for brevity, to capture the unmodeled dynamics of x_t, see Fig. 1. The dynamics vector $d_{t,t-1}$ incorporates the changes to the steady-state parameters (e.g., due to an unforeseen velocity) and is of the same dimension and unit as x_t. This completes the state transition, Eq. (14), to the *time-update equations*, with the corresponding VCM included, [28]

$$\begin{aligned} \underline{\hat{x}}_{t|t-1} &= \Phi_{t,t-1}\, \underline{\hat{x}}_{t-1|t-1} + \underline{d}_t, \\ Q_{\hat{x}_{t|t-1}} &= \Phi_{t,t-1}\, Q_{\hat{x}_{t-1|t-1}}\, \Phi_{t,t-1}^{\top} + Q_{d_t}, \end{aligned} \tag{15}$$

where $\underline{\hat{x}}_{t|t-1}$ is the *predicted state vector*, given the measurements up until $t-1$.

Without any further constraints, it would be impossible to infer or estimate the dynamics vector, and it would be impossible to distinguish measurement errors from actual physical motion. One effective constraint is to impose a level of temporal correlation (smoothness) in the physical behavior. Here we assume an exponentially correlated instantaneous velocity, using an Ornstein-Uhlenbeck process [29], leading subsequently to a temporally 'smooth' behavior in position

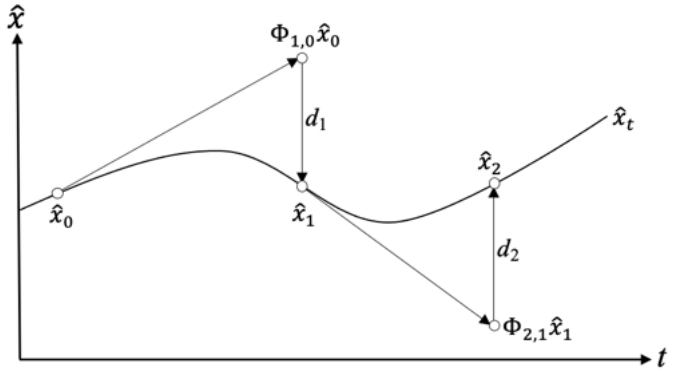

Fig. 1: A schematic diagram of the state transition $\hat{x}_t = \Phi_{t,t-1}\hat{x}_{t-1} + d_t$, where x represents a four-dimensional hyperspace with the four unknown parameters of Eq. (12). In the time-update equation, the transition matrix $\Phi_{t,t-1}$ predicts the new position in the hyperspace, while the dynamics vector d_t 'closes' the difference between the prediction and the true position in the hyperspace x_t.

[28], see App. VI. It is assumed to follow a zero-mean Gaussian distribution and can thus be characterized by the auto-covariance function,

$$C_v(\Delta t) = \sigma_v^2 e^{-\Delta t/\tau} \;\; \text{with } \tau > 0, \tag{16}$$

where Δt is the time interval between two epochs. The function is defined by

1) the standard deviation of the instantaneous velocity σ_v, and
2) the decorrelation time of the instantaneous velocity τ.

These two parameters describe the velocity behavior of the expected displacement signal and should either be defined a priori through expert elicitation, or determined based on empirical experience. They are important as they ultimately define the expected smoothness of the time series, i.e., including the admissible integer phase ambiguities. The standard deviation of the instantaneous velocity σ_v describes the magnitude of the steady-state behavior. If the signal is relatively steady, this value will be small (e.g., σ_v = 0.1 mm/yr), indicating a globally smooth signal with a small trend. In contrast, in areas with variable sub-surface dynamics, the value will be larger (e.g., σ_v = 20 mm/yr), reflecting a globally rough signal with a large trend.

As illustrated in Fig. 2, the exponential autocorrelation is presented as a function of the time interval, Δt, for decorrelation times τ of 30, 90, and 1000 days, respectively. The correlation corresponding to a given decorrelation time τ is $e^{-1} \approx 0.37$. By using Eq. (16), we assume that the velocity at a given time is statistically related to its past values, and this dependence decays exponentially with time. A longer decorrelation time results in a slower decay, hence, a locally smoother signal. A shorter decorrelation time indicates that the velocity varies more rapidly, which suggests a locally rougher signal. Thus, different combinations of (σ_v, τ) result in varying

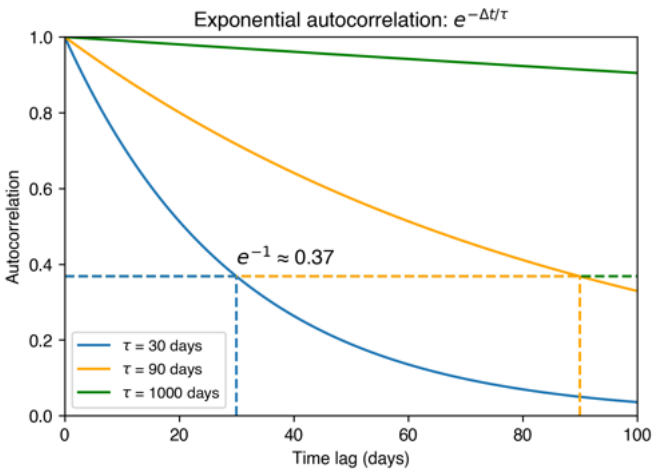

Fig. 2: Exponential autocorrelation of the instantaneous velocity as a function of Δt for decorrelation times (τ) of 30, 90, and 1000 days. Notably, the correlation reaches e^{-1} (≈ 0.37) when $\Delta t = \tau$.

TABLE I: The effect of σ_v and τ on the trend and smoothness of the signal. The terms 'small' and 'large' for σ_v and 'short' and 'long' for τ are relative rather than absolute.

	Short τ	Long τ
Small σ_v	Small trend; globally smooth; locally rough	Medium trend; globally smooth; locally smooth
Large σ_v	Medium trend; globally rough; locally rough	Large trend; globally rough; locally smooth

overall trends as well as global and local smoothness, see TABLE. I.

The transition matrix $\Phi_{t,t-1}$ can now be expressed as (see App. VI) [28]

$$\Phi_{t,t-1} = \begin{bmatrix} 1 & \tau\left(1 - e^{-\Delta t/\tau}\right) & 0 & 0 \\ 0 & e^{-\Delta t/\tau} & 0 & 0 \\ 0 & 0 & 1 & 0 \\ 0 & 0 & 0 & 1 \end{bmatrix}. \tag{17}$$

The transition model for exponentially correlated velocity includes $e^{-\Delta t/\tau}$ as an entry, representing the correlation function. As the time step Δt becomes much larger than τ, this value approaches zero, causing the velocity to effectively decorrelate and converge to the expected value—zero. ΔH and μ, cf. Eq. (12), are assumed to remain constant over time, resulting in zero variance for those components of the dynamics vector.

Without prior knowledge, the dynamics vector $\underline{d}_t$ is assumed to be zero. The stochasticity of d_t, Q_{d_t}, which implicitly contains the expected smoothness of the displacement signal, is given by [28]

$$Q_{d_t} = \sigma_v^2 \begin{bmatrix} q_{11} & & & sym. \\ q_{21} & q_{22} & & \\ 0 & 0 & 0 & \\ 0 & 0 & 0 & 0 \end{bmatrix} \tag{18}$$

with (see App. VI for derivation)

$$\begin{aligned} q_{11} &= 2\tau\left[\Delta t - \frac{3\tau}{2} + 2\tau e^{-\Delta t/\tau} - \frac{\tau}{2}e^{-2\Delta t/\tau}\right], \\ q_{21} &= 2\tau\left[-e^{-\Delta t/\tau} + \frac{1}{2}\left(1 + e^{-2\Delta t/\tau}\right)\right], \\ q_{22} &= \left[1 - e^{-2\Delta t/\tau}\right], \end{aligned}$$

where *sym.* indicates a symmetric matrix, and Δt indicates the absolute time difference between epoch t and $t-1$. These matrices are then used in the *time-update equation*, see Eq. (15). As a result of the assumption of a constant velocity in the initialization, the initial value for velocity, to initialize the recursive equations, is assumed to be zero with the predefined variance σ_v^2.

Once the prediction $\hat{x}_{t|t-1}$ is obtained, see Eq. (15), the *updated state vector* $\hat{x}_{t|t}$ and the corresponding VCM $Q_{\hat{\underline{x}}_{t|t}}$ can be computed by including the new observation $\underline{\phi}_t$ using the *measurement-update equation* [28],

$$\begin{aligned} \hat{\underline{x}}_{t|t} &= \hat{\underline{x}}_{t|t-1} + Q_{\hat{x}_{t|t}}\mathbf{A_t}^\top Q_{\phi_t}^{-1}\left(\underline{\phi}_t - \mathbf{A_t}\hat{x}_{t|t-1}\right); \\ Q_{\hat{x}_{t|t}} &= \left(Q_{\hat{x}_{t|t-1}}^{-1} + \mathbf{A_t}^\top Q_{\phi_t}^{-1}\mathbf{A_t}\right)^{-1}. \end{aligned} \tag{19}$$

Hence, the *updated state vector* $\hat{\underline{x}}_{t|t}$ is a weighted sum of the *predicted state vector* and the new observation, and can subsequently be used for predicting $\hat{\underline{x}}_{t+1|t}$ via the *time-update equation* (15).

The recursive equations would be straightforward when the absolute DD phases, $\underline{\phi}_t$, are known, see Eq. (19). Yet, as all observations are inherently wrapped modulo 2π, we make an assumption about the *predicted residual* between the absolute phase observation and its corresponding prediction at each epoch. Specifically, the *predicted residual* is defined as

$$\Delta\phi_t = \underline{\phi}_t - \mathbf{A_t}\hat{\underline{x}}_{t|t-1}. \tag{20}$$

It is assumed that this *predicted residual* lies within half a wave cycle, i.e., a quarter of the radar wavelength, such that

$$|\Delta\phi_t| < \pi. \tag{21}$$

The *predicted residual* then can be written as

$$\Delta\phi_t = \mathcal{W}\{\underline{\varphi}_t - A_t\hat{\underline{x}}_{t|t-1}\}. \tag{22}$$

where $\mathcal{W}$ is the modulo 2π operator, in this case transforming $\Delta\phi_t$ to the [-π, π) interval. Under this condition, the *measurement-update* Eq. (19) can be written as

$$\begin{aligned} \hat{\underline{x}}_{t|t} &= \hat{\underline{x}}_{t|t-1} + Q_{\hat{x}_{t|t}}\mathbf{A_t}^\top Q_{\varphi_t}^{-1}\mathcal{W}\left\{\underline{\varphi}_t - \mathbf{A_t}\hat{x}_{t|t-1}\right\}; \\ Q_{\hat{x}_{t|t}} &= \left(Q_{\hat{x}_{t|t-1}}^{-1} + \mathbf{A_t}^\top Q_{\varphi_t}^{-1}\mathbf{A_t}\right)^{-1}. \end{aligned} \tag{23}$$

This implies that the absolute phase $\underline{\phi}_t$ can be unambiguously resolved with Eqs. (20) and (22).

B. Processing scheme

The processing scheme of Dynamite is aimed at InSAR arcs, see Fig. 3. The process begins with a set of SLC data (referred to as 'daughters') coregistered to a common reference ('mother') SLC, from which the reference phase and DEM phase are removed to derive the temporal single-difference observations. For a specific PS j relative to a base PS i, we perform complex multiplication to obtain the spatio-temporal DD phase observation $\underline{\varphi}_t$ of the arc.

If the amplitude of a scatterer changes abruptly and significantly, we expect that the corresponding value of σ_ϕ may have changed as well. To account for this, we divide the time series into multiple partitions, each exhibiting its own distinct behavior, using the Pruned Exact Linear Time (PELT) algorithm, which optimizes the segmentation by minimizing a cost function plus a penalty term based on the statistical properties of the time series (e.g., mean or variance) [30]. Provided that there are sufficient observations within each partition, both the NMAD and consequently the phase quality can be estimated per partition [27]. We select partitions with a duration of at least half a year to account for potential seasonal variations in the amplitude behavior of the scatterers [27]. The observations are then divided into R partitions φ_{p_r} ($r = 1, 2, ..., R$) for the arc ij. We estimate the NMAD for each partition using Eq. (10), and approximate σ_ϕ with Eq. (11). The corresponding VCM $\mathbf{Q}_{\varphi_{\text{full}}}$ is then given by

$$\mathbf{Q}_{\varphi_{\text{full}}} = \bigoplus_{r=1}^{R} \left(\sigma^2_{\varphi_{p_r}} \mathbf{I}_{p_r} \right), \tag{24}$$

where $\bigoplus$ denotes the direct sum [31] forming a block diagonal matrix, $\sigma^2_{\varphi_{p_r}}$ is the standard deviation of the phase observations in partition p_r, and $\mathbf{I}_{p_r}$ is the identity matrix of size $n_{p_r} \times n_{p_r}$, with n_{p_r} being the number of observations in partition p_r.

Subsequently, in order to be able to evaluate and compare both approaches we implement both the batch and recursive processing method. In the batch processing, we apply ILS to resolve the ambiguities and estimate the parameters, see Eq. (5), using predefined standard deviations for the parameters (σ_S, σ_v, σ_{Δ_H}, σ_μ), considering both incremental and full time series. For the incremental approach, we use the time series $\varphi_{ij}^{1:t}$ where t is incrementally growing, starting with the initialization length I, and then subsequently concatenate with update epochs m_1+1, ..., m_1+m_2. The corresponding VCM is

$$\mathbf{Q}_{\varphi_{\text{inc}}} = \text{diag}\left(\sigma^2_{\varphi_{m_1}} \mathbf{I}_{m_1},\ \sigma^2_{\varphi_{m_1+1}},\ \sigma^2_{\varphi_{m_1+2}},\ \ldots,\ \sigma^2_{\varphi_t} \right), \tag{25}$$

where diag denotes a diagonal matrix, $\mathbf{I}_I$ is the identity matrix of size $m_1 \times m_1$, with I being the number of observations used in the initialization, $\sigma_{\varphi_{m_1}}$ and σ_{φ_t} (t = m_1+1, ..., m_1+m_2) denote the standard deviations of the phase observations during the initialization and at update epoch t of the incremental time series, respectively. These incremental time series and the corresponding VCM are used to estimate the unknowns $\underline{\hat{x}}_t$ (the same as b in Eq. (5)) and its corresponding VCM $Q_{\hat{x}_t}$ by Eq. (3). This is referred to as the incremental batch solution. For the full time series, when available, we can estimate a more accurate stochastic model using the VCM $Q_{\varphi_{\text{full}}}$, see Eq. (24), for the detected partitions. We then apply ILS again, incorporating partitioned quality estimation to estimate $\underline{\hat{x}}_{m_1+m_2}$ and $Q_{\hat{x}_{m_1+m_2}}$. This is referred to as the *full batch* solution.

In the recursive processing, see Fig. 4, we first apply ILS to the initial 50 epochs to obtain initial state vector estimates. We estimate the *predicted state vector* ($\underline{\hat{x}}_{t|t-1}$ and the VCM $Q_{\hat{x}_{t|t-1}}$) for the new epoch using the predefined standard deviation of velocity σ_v and the decorrelation time of velocity τ, and this is the time-update step. As a new observation becomes available, we then use the new wrapped phase ($\underline{\varphi}_t$) and the updated VCM, see Eqs. (10) and (11),

$$Q_{\varphi_t} = [\sigma^2_{\varphi_t}], \tag{26}$$

to adjust the predicted state vector, see Eq. (19). This measurement-update step yields the *updated state vector* ($\underline{\hat{x}}_{t|t}$, the VCM $Q_{\hat{x}_{t|t}}$) and the corresponding unwrapped phase ($\underline{\phi}_t$).

IV. Results and discussion

We demonstrate the recursive least-squares method to analyze nine years of Sentinel-1 data for a selected area of interest (AoI) in Amsterdam, the Netherlands. The recursive solution is compared to (i) the incremental batch solution as well as (ii) the full batch solution, where we chose one specific arc as example. Subsequently, we extend this comparison for all PS within the AoI, and investigate how the signal smoothness changes when the parameters of the exponentially correlated constraint vary. Finally, we assess the computational efficiency of the three approaches.

A. Batch and recursive solution

The processing approach sketched in Fig. 3 is applied. We select point scatterers (black dots in Fig. 5) with an NMAD smaller than 0.13, i.e., $\sigma_\varphi < 1$ mm, see Eq. (11), over the AoI, and the red and blue dots indicate the positions of PS i and PS j, respectively. Fig. 6 shows the amplitude and the corresponding NMAD of PS i (red) and PS j (blue). Fig. 6a shows the amplitude (dots) and the corresponding NMAD (solid line) and the detected partitions. The amplitude of PS j indicates anomalous behavior between 2017 and 2018, resulting in a partition with a greater NMAD. In Fig. 6b, the dashed lines show a constant batch-NMAD estimated using the full amplitude time series, while the solid lines show the 'retrospect' representation of NMAD, estimated from an incrementally growing amplitude time series. In other words, at each instant of time after initialization, this representation is computed using only the observations available in the present and past, i.e., it follows a causal system [32] that does not depend on future data or the entire time series. These retrospective-NMAD values are thus used for the incremental

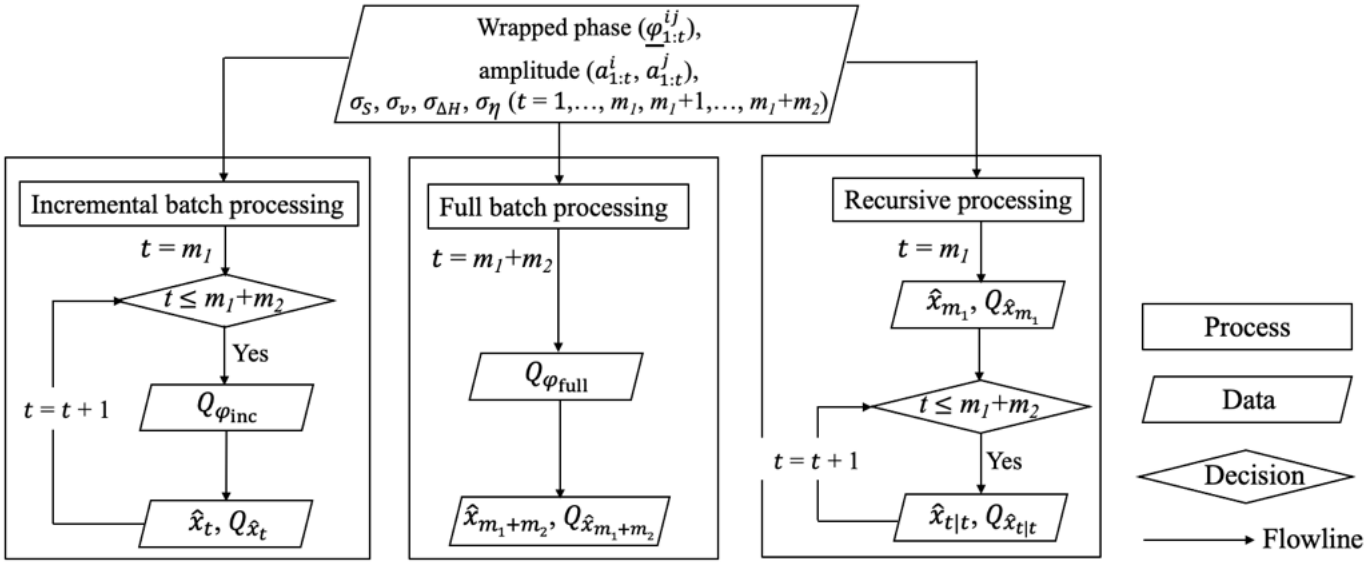

Fig. 3: Flowchart of parameter estimation with three options: the incremental batch solution, the full batch solution, and the proposed constrained recursive solution for an individual InSAR arc.

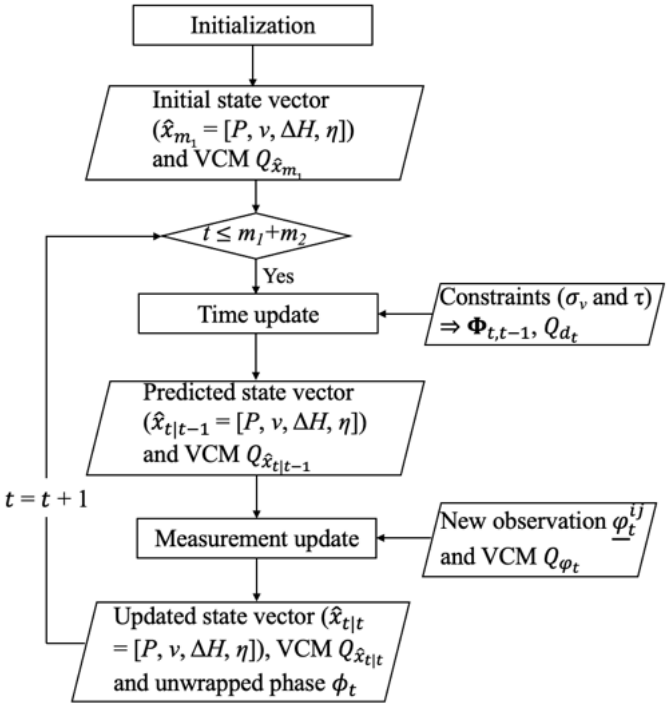

Fig. 4: Flowchart of recursive parameter estimation (right box of Fig. 3) for an individual InSAR arc.

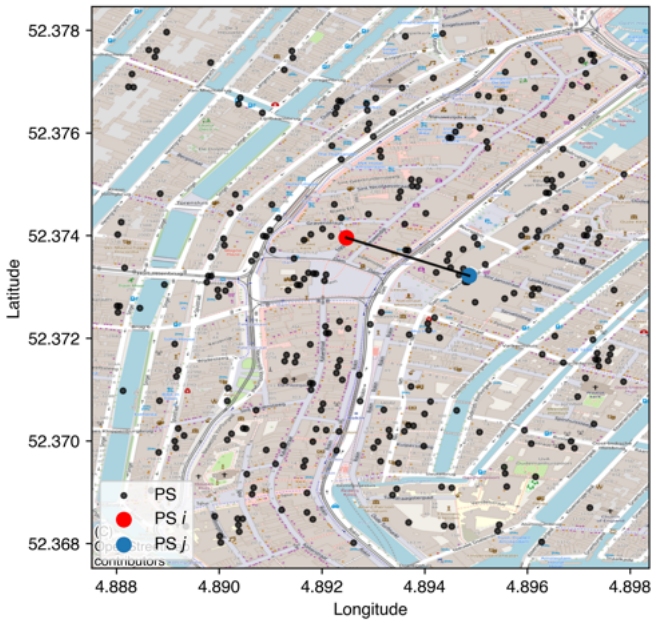

Fig. 5: The map of the AoI in Amsterdam, the Netherlands. The black dots represent the PS used in this study. The red and blue dots indicate the positions of PS i and PS j, respectively, while the black line between them indicates the arc.

batch solution and the recursive solution, respectively. For PS j, the retrospective-NMAD reaches a peak at the end of the detected anomalous partition between 2017 and 2018, after which it gradually retreats to a new asymptote.

Fig. 7 shows the solutions for the incremental batch, full batch, and recursive approaches for the selected arc connecting PS i and PS j. Fig. 7a presents the DD phase and the adjusted (estimated) DD phase for the three approaches. The batch solution (the blue line) completely misses the 2017-2018 anomaly, as it is tuned to estimate global static parameters. When applied incrementally (the green line) with a growing time series (i.e., the *retrospective* estimate at each epoch is only based on the available data up until that time) the solution lags behind the changes in 2017 and 2018, and it

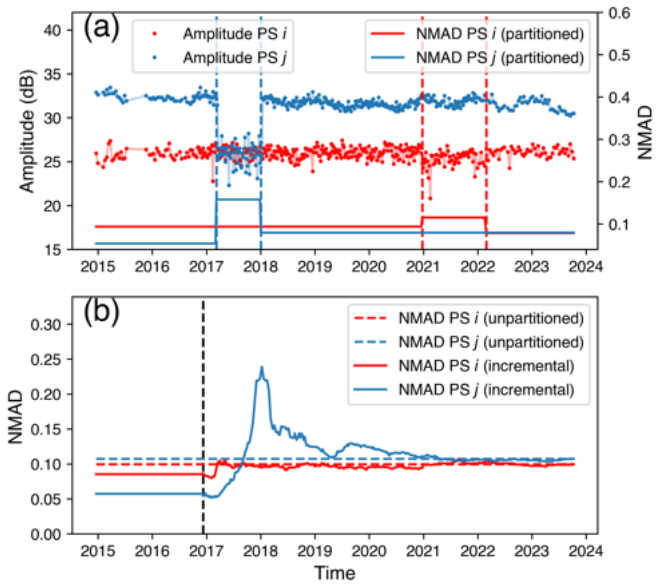

Fig. 6: Amplitude and NMAD of PS i and PS j of Fig. 5. (a) The left y-axis shows the amplitude of PS i (red) and PS j (blue), and the right y-axis shows the corresponding NMAD with detected partitions. (b) The dashed lines show the unpartitioned NMAD estimated using the full amplitude time series, and the solid lines show the retrospective NMAD estimated with the incremental amplitude time series. These NMAD are used for the incremental batch solution and the recursive solution.

takes about two extra years of data acquisitions to converge to the actual values. Clearly, the recursive approach (the orange line) fits the observations much better than the two batch approaches, and is able to quickly adapt to the changing circumstances. Note that the blue dots and the orange dots always coincide. This indicates that the adjusted, (i.e., 'unwrapped') recursive observations (orange dots) match with the adjusted, (i.e., 'unwrapped') full batch observations (blue dots). This suggests that the proposed ambiguity resolution assumption $|\Delta\phi_t| < \pi$, see Eq. (21) is reasonable. Fig. 7b illustrates the relative position, revealing that the linear model in the batch solutions fails to capture the anomalous signal, the incremental batch solution lags behind for two years, whereas the recursive solution effectively captures the non-linear displacements. Figs. 7c illustrates the instantaneous velocity. In the recursive solution, the instantaneous velocity is explicitly adopted in the functional model and is constrained with predefined parameters σ_v = 3 mm/yr and $\tau = 30$ days. It is important to stress that the instantaneous velocity is not derived through differentiation of the estimated relative positions, but treated as independent state variable and is estimated separately. This provides a comprehensive state estimation of the dynamic system. Figs. 7d and e show the estimated residual cross-range distance (dependent on the elevation of the scatterers) and thermal expansion factor, respectively, based

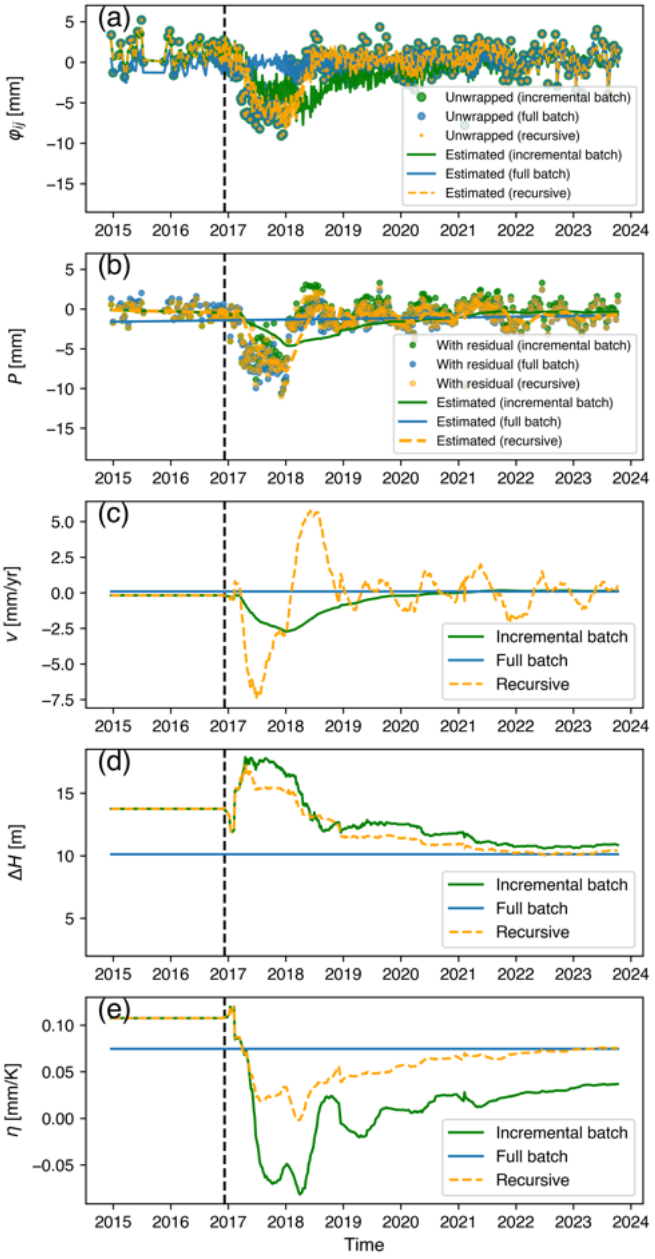

Fig. 7: Incremental batch solution (green), full batch solution (blue), and recursive solution (orange-dashed) of the arc shown in Fig. 5. (a) The DD phase and the adjusted DD phase; (b) The residual cross-range distance; (c) The thermal expansion factor of the arc; (d) The relative position; (e) The instantaneous velocity; The black dash lines in (a)–(e) show the last (50th) epoch of the initialization.

on the three approaches. Obviously, the full batch approach (blue) has the advantage of hindsight, i.e., the availability of all observations of the full time series. Thus these lines should not be interpreted sequentially, but their values can be interpreted as near-optimal, since they use all available data. In contrast, the results of the incremental batch and recursive approaches should be interpreted per epoch, based only on the retrospective information at that time. After initialization, the recursive approach (orange) performs better and faster than the incremental batch approach (green) in providing estimates comparable to the full batch solution, converging towards the full batch solution at the final epoch. In general, the recursive approach yields solutions of comparable quality to those of the full batch method, while effectively capturing the dynamic changes in the time series and operating without access to future data.

B. Spatial analysis

As shown in Fig. 5, 285 point scatterers with NMAD < 0.13 are selected. Among these, the point scatterer with the smallest NMAD, i.e., best expected phase quality, is chosen as the initial reference point (black star in Fig. 8). A total of 284 arcs are then generated between the reference point and the other point scatterers. The predefined parameters of the recursive solution are conservatively set to $\sigma_v = 3$ mm/yr and $\tau = 150$ days. The rows of Fig. 8 show: (a–c) the average LoS displacement rate v, (d–f) the residual cross-range distance ΔH, and (g–i) the thermal expansion factor η of these point scatterers relative to the reference point from the full batch solution (left), the recursive solution (middle), and their difference (right). The right column shows that most of the arcs have comparable results whether in full-batch or recursive, which demonstrates the compliance of our smoothness-constrained recursive method, the recursive method using a dynamic parameterization performs on par with the batch solution. The means of the differences of v, ΔH and η are -0.03 mm/yr, -0.02 m and 0.002 mm/K, respectively.

PS1–PS4 in Fig. 8c are four representative examples to illustrate the differences between the two estimation methods. Their corresponding instantaneous positions (P) over time, relative to the reference point, are shown in Fig. 9, where the full batch solution is depicted in blue and the recursive solution (i.e., retrospect representation) is displayed in orange. The displacement signal of PS1 (Fig. 9a) exhibits a noisier episode since mid-2020, alongside fluctuations in the time series behavior. The recursive solution is more likely to adjust effectively to these observations, while the batch solution exhibits more frequent cycle slips after mid-2020, which result in undesirable unwrapping errors. For PS2 (Fig. 9b), the behavior changes around mid-2019. The recursive solution adapts to this shift and captures the evolving dynamics, while the batch solution fails to reflect it, as its parameters remain numerically unchanged by definition. Fig. 9c illustrates that while the difference between the two methods for PS3 is limited, the recursive solution is able to capture its dynamic behavior better, particularly the uplift observed in early 2018. In Fig. 9d, PS4 experienced a displacement change in early 2018. Following this change, the two approaches exhibit distinct unwrapping solutions. The recursive solution shifts to a different ambiguity level, while the batch solution yields a result with one fewer ambiguity level, and this will be further elaborated in Sec. IV-C. These examples suggest that while a different method cannot claim to be 'correct', the recursive solution, which does not have the full-batch benefit of hindsight, performs equally well.

C. Influence of the smoothness constraints

Given the distinct ambiguity resolution results produced by the batch and recursive solutions for PS4 (Fig. 9d), we use this example to investigate the influence of the smoothness constraints on the signal. Fig. 10 shows the position (P) of PS4 relative to the reference point shown in Fig. 9d with different constraints. Fig. 10a is the same as the recursive solution in Fig. 9d, i.e., the default solution. Increasing σ_v (Figs. 10a and b) or τ (Figs. 10a and c) introduces more flexibility into the signal, allowing the model to respond more quickly to changes in the dynamic behavior. In addition, Figs. 10b and c demonstrate that relatively small values of σ_v or τ yield results that more closely align with the conventional linear model, due to the more limited range of permissible variations. In Fig. 10d, the model more quickly captures the variation around 2018 compared to the solution in Fig. 10a, thus the smoothness parameters can be tuned to better capture the dynamics in the behavior. It is worth noting that similar results can arise from different combinations of σ_v and τ, as illustrated in Figs.10a and d, as well as b and c. Conversely, variations in either σ_v or τ can also lead to distinct outcomes. As a result, ambiguity resolution is inherently controlled by the predefined parameters σ_v and τ, leading to *implicit phase unwrapping*.

It is important to stress that the smoothness constraints are not parameters that need to be estimated from the data. Rather, they are based on prior expectations of the dynamic behavior of the objects in the AoI. As such, the choice for the values of the smoothness constraints is comparable to the choice of estimating a particular parametric model (e.g., 'linear plus sinusoidal') in conventional batch estimation.

D. Computational efficiency

We evaluate the computation efficiency for the three approaches based on individual arcs. For the recursive approach, the computation effort for each updated epoch remains consistent, regardless of the length of the time series up to that epoch. Consequently, its computational complexity is $O(T)$, where T represents the number of epochs. It is a linear function since the solution at each epoch is derived directly from the previous epoch, requiring only a single iteration.

Both the incremental batch and full batch solutions show a computational complexity of $O(T^3)$. This cubic complexity arises from the need to solve a system of equations involving all available epochs each time a new observation is introduced. As the number of epochs increases, this approach results in a substantial escalation in computational cost.

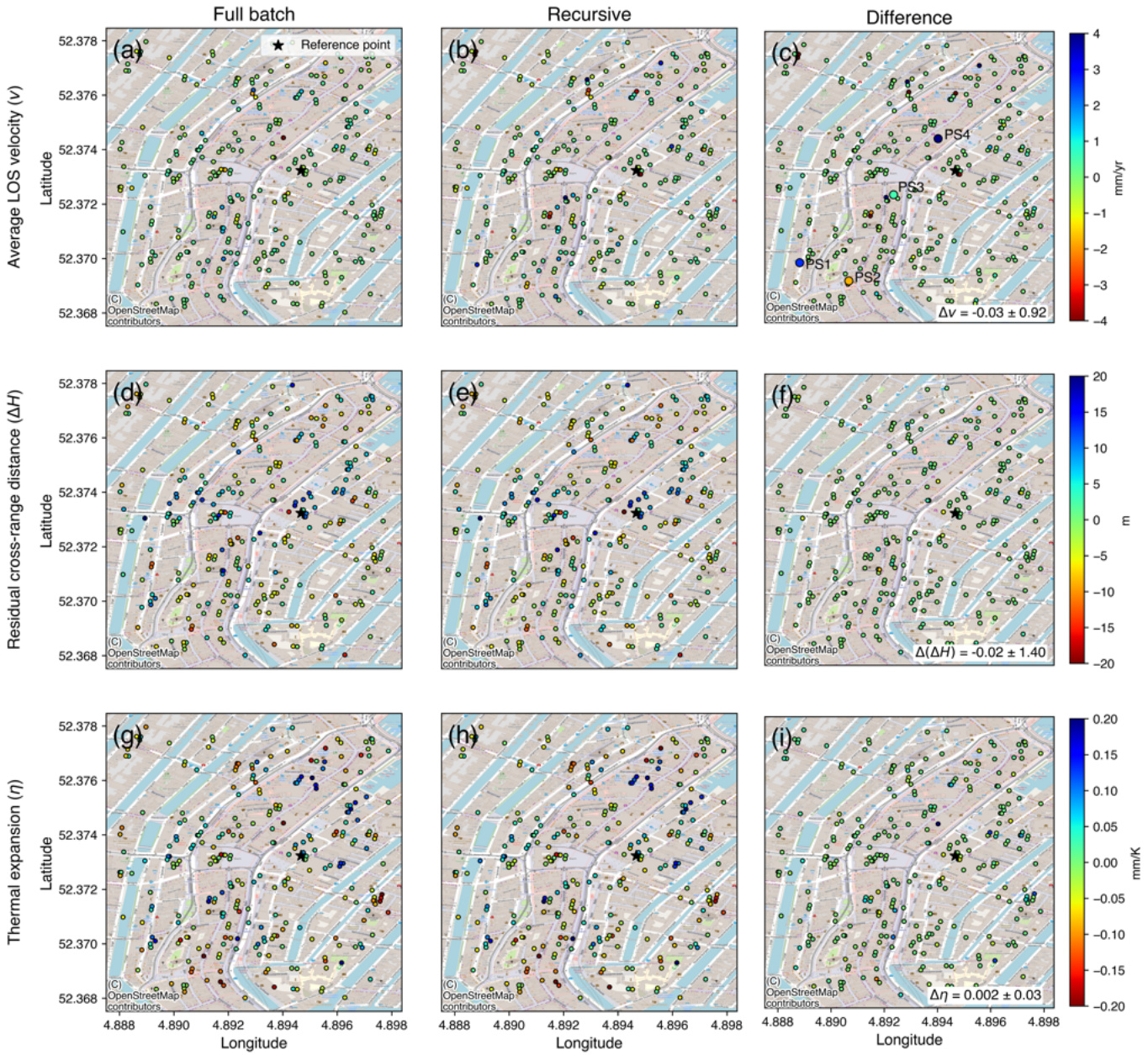

Fig. 8: Estimated parameters for the full batch solution (column 1), the recursive solution (column 2), and their difference (column 3). First row (a–c): displacement rate v . Second row (d–f): residual cross-range distance ΔH. Third row (g–i): thermal expansion factor η. The recursive solutions for ΔH and η are the hindsight-estimates from the last epoch of the time series. The predominance of green dots in the third column indicates that the recursive solution on par with the full batch solution. In (c), PS1, PS2, PS3 and PS4 show a relatively large difference in the two solutions. Their displacement time series are shown in Fig. 9.

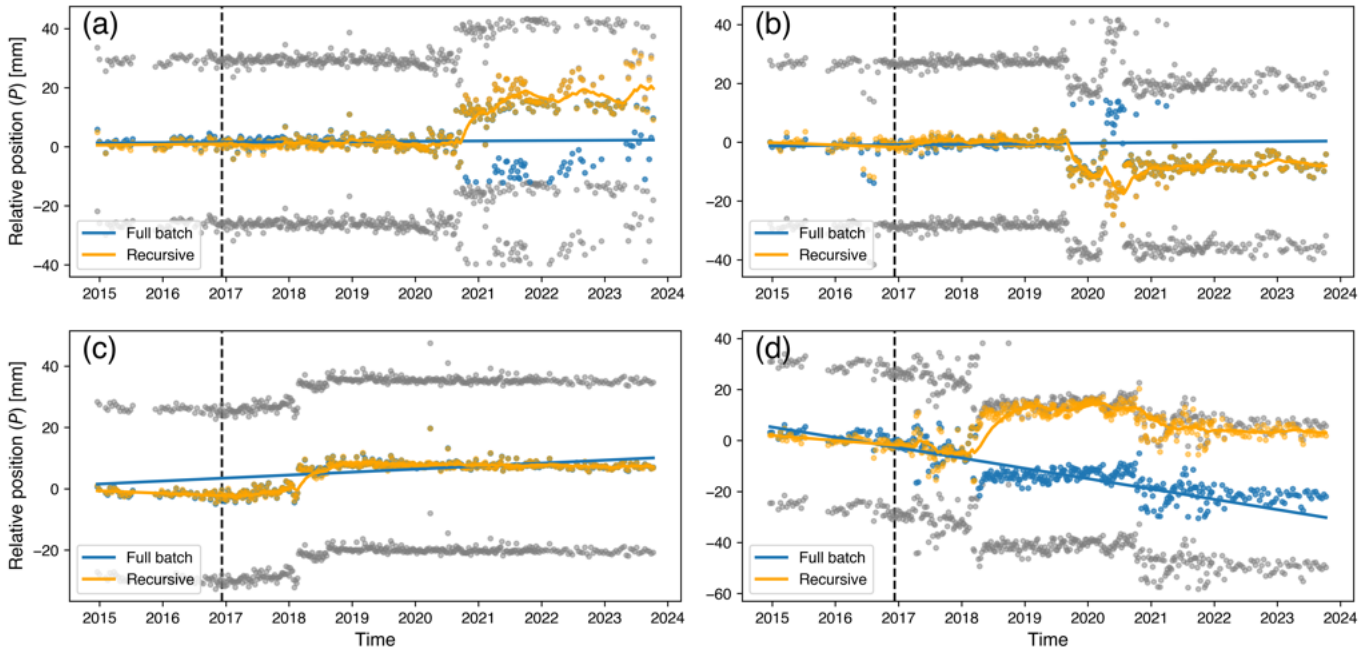

Fig. 9: Estimated relative positions P of PS1–PS4 (cf. Fig. 8c) relative to the reference point. The blue line model reflects the hindsight batch constant velocity model, while the orange line represents the instantaneous relative position, only based on retrospective observations, i.e., for each epoch looking back in time. (a) PS1: the quality and behavior of the time series fluctuated since mid-2020. The recursive method is able to adjust its estimates accordingly, while the batch method fails to do so, resulting in potential unwrapping errors. (b) PS2: a change in behavior is observed around mid-2019. The recursive solution seems to reflect the dynamics of the point more accurately, whereas the batch estimation lacks the flexibility to adapt to the change. (c) PS3: the recursive solution seems to be more representative in capturing the actual dynamic behavior of the point. (d) PS4: the two solutions diverge, exhibiting distinct behaviors in early 2018.

From a monitoring perspective in an urban setting, millions of point scatterers require updating whenever a new acquisition becomes available, resulting in a substantial increase in computational cost due to the growing number of epochs for the batch solution. In contrast, the recursive solution efficiently updates each scatterer by directly utilizing the estimates from the previous epoch, minimizing redundant calculations.

V. Conclusion

The integration of recursive least-squares with smoothness constraints offers a robust framework for dynamic parameter estimation of InSAR scatterer motion in near-real time (DYNAMITE). It reduces the dependency on an a priori static parameterization, and allows for the independent temporal behavior of each scatterer to be more accurately captured.

The recursive solution demonstrates performance on par with the full batch solution in the studied case, with significantly higher computational efficiency and a reduced risk of ambiguity errors. Despite its distinct approach, the recursive method maintains accuracy without underperforming compared to the batch solution. Moreover, it effectively captures dynamic behavior, particularly displacement anomalies. The dynamic parameterization is not designed to fit a model to the data but to describe the actual motion of a point, independent of the measurements.

The chosen exponentially correlated velocity model incorporates an explicit smoothness constraint on the displacement signal by defining two input parameters: the standard deviation of the velocity σ_v and the decorrelation time of the velocity τ. As different values of the two smoothness parameters may lead to different integer phase ambiguity solutions, this method can be regarded as *implicit* phase unwrapping. It is important to stress that these smoothness parameters are *not* derived from the InSAR data but are intrinsic characteristics of the motion of the points being analyzed. A smaller σ_v indicates a globally smooth signal with a relatively small overall trend, whereas a larger σ_v allows for greater amplitude variations, suggesting a globally rough signal with a more pronounced trend. A longer decorrelation time τ implies that the velocity persists over a longer duration, resulting in a locally smoother signal. In contrast, a shorter τ reflects more localized variations, indicating a locally rougher signal. Yet, while the choice of smoothness parameters is critical, it shows not to be overly restrictive. For effective anomaly detection, these parameters should be set conservatively, as loose smoothness assumptions could hamper the detection of actual motion. In the case study conducted in Amsterdam, we set $\sigma_v = 3$ mm/yr^2 and $\tau = 150$ days for parameter estimation. Under these settings, the mean differences in v, ΔH and η relative to the full batch solution

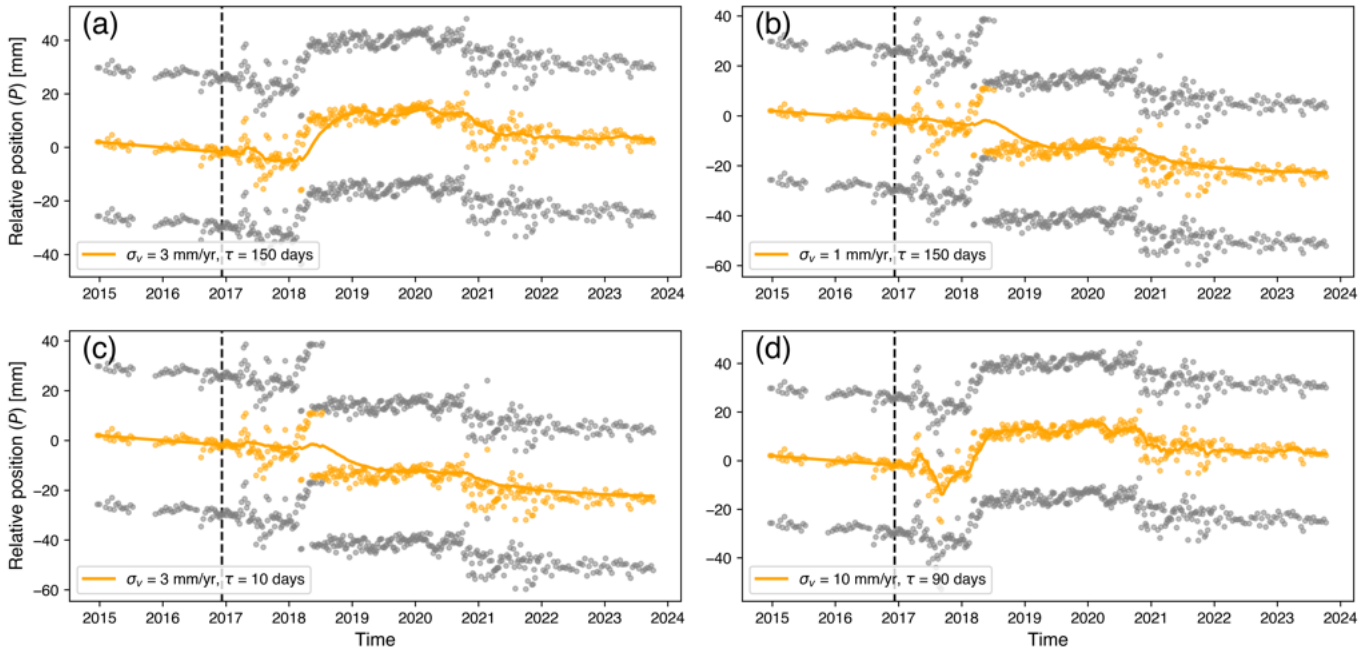

Fig. 10: Influence of the smoothness constraints on the signal for PS4 relative to the reference point shown in Fig. 8(d). (a)-(c) The position with constraints $[\sigma_v,\ \tau]$ = $[3, 150]$ (default) (a), $[1, 150]$ (b), $[3, 10]$ (c) and $[10, 90]$ in [mm/yr] and [days]. The gray dots in (a)-(d) indicate the ± 1 ambiguity levels. The different solutions indicates the choice of the smoothness parameters enables the implicit phase unwrapping.

are -0.03 mm/yr, -0.02 m and 0.002 mm/K, respectively, suggesting that the results are comparable to those of the full batch solution. This establishes a framework for testing the estimated parameters and issuing early warnings of potential anomalies.

Both the incremental and full batch solutions exhibit a computational complexity of $O(T^3)$, causing significant computational costs as the number of epochs increases. In contrast, the recursive solution, with a computational complexity of $O(T)$, efficiently updates scatterers using prior estimates, significantly improving computational efficiency.

VI. Appendix: Exponentially Correlated Velocity

In Section III-A temporal correlation was introduced as a smoothness constraint in the state transitions. This constraint is inferred on $\Phi_{t,t-1}$ and d_t in the *time-update*, Eq. (15). Below, we clarify the rationale for employing an exponentially correlated velocity model in the state transition and derive the variance-covariance matrix Q_{d_t}. Our approach is based on the assumption that the velocity at a given time is statistically related to its past values, and this dependence decays exponentially with time difference, using an exponentially correlated zero-mean velocity model proposed by Teunissen [28].

An exponentially correlated random function can be characterized as the solution to a first-order stochastic differential equation driven by white noise, i.e., an Ornstein-Uhlenbeck process [29] to describe velocity. This means the velocity has memory (temporal correlation), but this memory fades exponentially, and over time the process tends to drift towards its mean function, i.e., it is *mean-reverting*. Consequently, we define the zero-mean velocity v_t by the differential equation [28]:

$$\dot{v}_t = -\lambda v_t + z(\zeta), \tag{27}$$

with

$$\begin{aligned} \sigma_{zz}(\zeta) &= 2\lambda\sigma_v^2\delta(\zeta) \ \text{ (white noise)} \\ \sigma_{v_{t_0}^2} &= \sigma_v^2 \\ \sigma_{(Dv)_{t_0}} &= 0,\ \sigma_{(vz)_{t_0}} = 0,\ \forall t \\ E\left\{\underline{v}_{t_0}\right\} &= 0,\ E\{\underline{v}_t\} = 0,\ \forall t \end{aligned} \tag{28}$$

where $\lambda > 0$ is the correlation decay rate or damping function (greater λ = faster decay), $\delta(\zeta)$ is the Dirac delta function and $\int_{-\infty}^{\infty}\delta(\zeta)d\zeta = 1$. We use the decorrelation time $\tau = 1/\lambda$ (i.e., greater decorrelation time = slower decay) in this study.

Following Eq. (27), the state vector x_t, see Eq. (12), can be described by the following differential equation:

$$\underbrace{\begin{bmatrix} \dot{D}_t \\ \dot{v}_t \\ \dot{\Delta H}_t \\ \dot{\eta}_t \end{bmatrix}}_{\dot{\underline{x}}_t} = \underbrace{\begin{bmatrix} 0 & 1 & 0 & 0 \\ 0 & -\lambda & 0 & 0 \\ 0 & 0 & 0 & 0 \\ 0 & 0 & 0 & 0 \end{bmatrix}}_{F} \underbrace{\begin{bmatrix} D_t \\ v_t \\ \Delta H_t \\ \eta_t \end{bmatrix}}_{\underline{x}_t} + \underbrace{\begin{bmatrix} 0 \\ 1 \\ 0 \\ 0 \end{bmatrix}}_{G} z_t. \tag{29}$$

Its unique solution is given by [28]

$$x_t = e^{F\Delta t}x_{t_0} + \int_{\zeta=t_0}^{t} e^{F(t-\zeta)}\, G\, z(\zeta)d\zeta, \tag{30}$$

where $\Delta t = t - t_0$. The epoch t_0 can be adjusted to epoch $t-1$ in the context of the recursive update, i.e.,

$$x_t = e^{F\Delta t} x_{t-1} + \int_{\zeta=t-1}^{t} e^{F(t-\zeta)}\, G\, z(\zeta) d\zeta, \qquad (31)$$

where Δt indicates the absolute time difference between epoch t and $t-1$. This solution is equivalent to the *time-update equation*, see Eq. (15), and the transition matrix $\Phi_{t,t-1}$, see Eq. (17), corresponds with $e^{F\Delta t}$, i.e.,

$$\Phi_{t,t-1} = e^{F\Delta t} = \begin{bmatrix} 1 & \tau\left(1 - e^{-\frac{\Delta t}{\tau}}\right) & 0 & 0 \\ 0 & e^{-\frac{\Delta t}{\tau}} & 0 & 0 \\ 0 & 0 & 1 & 0 \\ 0 & 0 & 0 & 1 \end{bmatrix}. \qquad (32)$$

With Eqs. (28) and (31), the stochasticity of d_t expressed by Q_{d_t}, see Eq. (18), is given by [28]

$$\begin{aligned} Q_{d_t} &= \int_{\zeta=t-1}^{t} \frac{2\sigma_v^2}{\tau} (e^{F(t-\zeta)})^\top\, G^\top\, G\, e^{F(t-\zeta)} d\zeta \\ &= \sigma_v^2 \begin{bmatrix} q_{11} & & & sym. \\ q_{21} & q_{22} & & \\ 0 & 0 & 0 & \\ 0 & 0 & 0 & 0 \end{bmatrix}, \end{aligned} \qquad (33)$$

elaborated further in Eq. (18).

REFERENCES

[1] R. F. Hanssen, *Radar Interferometry: Data Interpretation and Error Analysis*. Dordrecht: Kluwer Academic Publishers, 2001.

[2] A. Ferretti, C. Prati, and F. Rocca, "Permanent Scatterers in SAR Interferometry," *IEEE Trans Geosci Remote Sens*, vol. 39, no. 1, pp. 8–20, 2001.

[3] F. J. van Leijen and R. F. Hanssen, "Persistent scatterer density improvement using adaptive deformation models," in *2007 IEEE International Geoscience and Remote Sensing Symposium*, 2007, pp. 2102–2105.

[4] F. J. van Leijen, "Persistent Scatterer Interferometry based on geodetic estimation theory," Ph.D. dissertation, Delft University of Technology, 2014.

[5] P. Conroy, S. A. N. van Diepen, S. Van Asselen, G. Erkens, F. J. van Leijen, and R. F. Hanssen, "Probabilistic estimation of insar displacement phase guided by contextual information and artificial intelligence," *IEEE Transactions on Geoscience and Remote Sensing*, vol. 60, pp. 1–11, 2022.

[6] Y. Wang, W. S. Brouwer, F. J. Van Leijen, and R. F. Hanssen, "Non-Parametric InSAR Time Series Analysis of Arcs Using Complex B-Splines," in *IGARSS 2023 - 2023 IEEE International Geoscience and Remote Sensing Symposium*, 2023, pp. 8238–8241.

[7] Y. Wang, W. S. Brouwer, F. J. van Leijen, and R. F. Hanssen, "Constrained recursive parameter estimation for insar arcs," in *IGARSS 2024 - 2024 IEEE International Geoscience and Remote Sensing Symposium*, 2024, pp. 10 689–10 693.

[8] L. Chang and R. F. Hanssen, "A Probabilistic Approach for InSAR Time-Series Postprocessing," *IEEE Transactions on Geoscience and Remote Sensing*, vol. 54, no. 1, pp. 421–430, 2016.

[9] P. S. Marinkovic, F. van Leijen, G. Ketelaar, and R. F. Hanssen, "Recursive data processing and data volume minimization for PS-InSAR," in *IGARSS 2005 - 2005 IEEE International Geoscience and Remote Sensing Symposium*, vol. 4, 2005, pp. 2697–2700.

[10] F. Xue and X. Lv, "Applying time series interferometric synthetic aperture radar and the unscented Kalman filter to predict deformations in Maoxian landslide," *Journal of Applied Remote Sensing*, vol. 13, no. 01, p. 1, 2019.

[11] B. Wang, C. Zhao, Q. Zhang, Z. Lu, Z. Li, and Y. Liu, "Sequential Estimation of Dynamic Deformation Parameters for SBAS-InSAR," *IEEE Geoscience and Remote Sensing Letters*, vol. 17, no. 6, pp. 1017–1021, 2020.

[12] J. Liu, J. Hu, Z. Li, Q. Sun, Z. Ma, J. Zhu, and Y. Wen, "Dynamic Estimation of Multi-Dimensional Deformation Time Series from InSAR Based on Kalman Filter and Strain Model," *IEEE Transactions on Geoscience and Remote Sensing*, vol. 60, pp. 1–16, 2022.

[13] J. Cai, G. Liu, H. Jia, B. Zhang, R. Wu, Y. Fu, W. Xiang, W. Mao, X. Wang, and R. Zhang, "A new algorithm for landslide dynamic monitoring with high temporal resolution by Kalman filter integration of multiplatform time-series InSAR processing," *International Journal of Applied Earth Observation and Geoinformation*, vol. 110, 2022.

[14] Q. Verburg, "QUInSAR: Temporal Parameter and Ambiguity Estimation Using Recursive Least-Squares: A Methodology for Persistent Scatterer Interferometry," MSc. thesis, TU Delft, the Netherlands, 2017.

[15] H. Ansari, F. De Zan, and R. Bamler, "Sequential Estimator: Toward Efficient InSAR Time Series Analysis," *IEEE Transactions on Geoscience and Remote Sensing*, vol. 55, no. 10, pp. 5637–5652, 2017.

[16] M. Dalaison and R. Jolivet, "A Kalman Filter time series analysis method for InSAR," *Journal of Geophysical Research : Solid Earth*, pp. 1–21, 2020.

[17] F. Hu, F. J. van Leijen, L. Chang, J. Wu, and R. F. Hanssen, "Combined Detection of Surface Changes and Deformation Anomalies Using Amplitude-augmented Recursive InSAR Time Series," *IEEE Trans Geosci Remote Sens*, vol. 60, pp. 1–16, 2022.

[18] A. Ferretti, A. Fumagalli, F. Novali, C. Prati, F. Rocca, and A. Rucci, "A New Algorithm for Processing Interferometric Data-Stacks: SqueeSAR," *IEEE Transactions on Geoscience and Remote Sensing*, vol. 49, no. 9, pp. 3460–3470, 2011.

[19] F. Hu, J. Wu, L. Chang, and R. F. Hanssen, "Incorporating temporary coherent scatterers in multi-temporal InSAR using adaptive temporal subsets," *IEEE transactions on geoscience and remote sensing*, vol. 57, no. 10, pp. 7658–7670, 2019.

[20] P. Conroy, S. A. N. van Diepen, F. J. van Leijen, and R. F. Hanssen, "Bridging loss-of-lock in insar time series of distributed scatterers," *IEEE Transactions on Geoscience and Remote Sensing*, vol. 61, pp. 1–11, 2023.

[21] P. J. G. Teunissen, "Least-Squares Estimation of the Integer GPS Ambiguities," in *Invited Lecture, Section IV Theory and Methodology, the General Meeting of the International Association of Geodesy, Beijing, China*, August 1993.

[22] B. Kampes and R. F. Hanssen, "Ambiguity resolution for permanent scatterer interferometry," *Geoscience and Remote Sensing, IEEE Transactions on*, vol. 42, no. 11, pp. 2446–2453, Nov 2004.

[23] P. J. G. Teunissen, "The least-squares ambiguity decorrelation adjustment: a method for fast GPS integer ambiguity estimation," *Journal of Geodesy*, vol. 70, pp. 65–82, 1995.

[24] H. Fattahi and F. Amelung, "DEM Error Correction in InSAR Time Series," *IEEE Transactions on Geoscience and Remote Sensing*, vol. 51, no. 7, pp. 4249–4259, 2013.

[25] L. Chang, R. P. B. J. Dollevoet, and R. F. Hanssen, "Nationwide railway monitoring using satellite sar interferometry," *IEEE Journal of Selected Topics in Applied Earth Observations and Remote Sensing*, vol. 10, no. 2, pp. 596–604, 2017.

[26] W. S. Brouwer, Y. Wang, F. J. van Leijen, and R. F. Hanssen, "On the Stochastic Model for InSAR Single Arc Point Scatterer Time Series," in *IGARSS 2023 - 2023 IEEE International Geoscience and Remote Sensing Symposium*, 2023, pp. 7902–7905.

[27] W. S. Brouwer and R. F. Hanssen, "On the Definition of an Independent Stochastic Model for InSAR Time Series," *IEEE Transactions on Geoscience and Remote Sensing*, 2025 (under review).

[28] P. J. G. Teunissen, *Dynamic data processing: Recursive least-squares*, 1st ed. Delft: Delft University Press, 2001.

[29] G. E. Uhlenbeck and L. S. Ornstein, "On the theory of the brownian motion," *Phys. Rev.*, vol. 36, pp. 823–841, Sep 1930. [Online]. Available: https://link.aps.org/doi/10.1103/PhysRev.36.823

[30] C. Truong, L. Oudre, and N. Vayatis, "Selective review of offline change point detection methods," *Signal Processing*, vol. 167, p. 107299, 2020.

[31] G. Strang, *Introduction to Linear Algebra*, 5th ed. Wellesley, MA: Wellesley-Cambridge Press, 2016.

[32] A. V. Oppenheim and G. C. Verghese, *Signals, systems & inference*. Pearson London, 2017.